Midrapidity Source of Intermediate-Mass Fragments in Highly Central Collisions of Au + Au at 150A MeV

J. P. Alard,[3] Z. Basrak,[13] N. Bastid,[3] I. M. Belayev,[8] M. Bini,[5] Th. Blaich,[7] R. Bock,[4] A. Buta,[1] R. Čaplar,[13] C. Cerruti,[11] N. Cindro,[13] J. P. Coffin,[11] M. Crouau,[3] P. Dupieux,[3] J. Erö,[2] Z. G. Fan,[4] P. Fintz,[11] Z. Fodor,[2] R. Freifelder,[4] L. Fraysse,[3] S. Frolov,[8] A. Gobbi,[4] Y. Grigorian,[9] G. Guillaume,[11] N. Herrmann,[6] K. D. Hildenbrand,[4] S. Hölbling,[13] O. Houari,[11] S. C. Jeong,[4] M. Jorio,[3] F. Jundt,[11] J. Kecskemeti,[2] P. Koncz,[2] Y. Korchagin,[8] R. Kotte,[10] M. Krämer,[4] C. Kuhn,[11] I. Legrand,[1] A. Lebedev,[8] C. Maguire,[11] V. Manko,[9] T. Matulewicz,[12] G. Mgebrishvili,[9] J. Mösner,[10] D. Moisa,[1] G. Montarou,[3] P. Morel,[3] W. Neubert,[10] A. Olmi,[5] G. Pasquali,[5] D. Pelte,[6] M. Petrovici,[1] G. Poggi,[5] F. Rami,[11] W. Reisdorf,[4] A. Sadchikov,[9] D. Schüll,[4] Z. Seres,[2] B. Sikora,[12] V. Simion,[1] S. Smolyankin,[8] U. Sodan,[4] N. Taccetti,[5] K. Teh,[4] R. Tezkratt,[11] M. Trzaska,[6] M. A. Vasiliev,[9] P. Wagner,[11] J. P. Wessels,[4] T. Wienold,[6] Z. Wilhelmi,[12] D. Wohlfarth,[10] and A. V. Zhilin[8]

[1]*Institute for Physics and Nuclear Engineering, Bucharest, Romania*
[2]*Central Research Institute for Physics, Budapest, Hungary*
[3]*Laboratoire de Physique Corpusculaire, Clermont-Ferrand, France*
[4]*Gesellschaft für Schwerionenforschung, Darmstadt, Germany*
[5]*Università and Istituto Nazionale di Fisica Nucleare, Florence, Italy*
[6]*Physikalisches Institut der Universität Heidelberg, Heidelberg, Germany*
[7]*Universität Mainz, Mainz, Germany*
[8]*Institute for Experimental and Theoretical Physics, Moscow, Russia*
[9]*Kurchatov Institute for Atomic Energy, Moscow, Russia*
[10]*Zentralinstitut für Kernforschung, Rossendorf, Germany*
[11]*Centre de Recherches Nucléaires and Université Louis Pasteur, Strasbourg, France*
[12]*Institute of Experimental Physics, Warsaw University, Warsaw, Poland*
[13]*Rudjer Boskovic Institute, Zagreb, Croatia*

(Received 3 February 1992; revised manuscript received 29 May 1992)

Charged particles have been observed in collisions of Au on Au at an incident energy of 150A MeV using a high-granularity detector system covering approximately the forward hemisphere in the center-of-mass system. Highly central collisions have been studied using a double selection criterion which combines large charged-particle multiplicities with small transverse-momentum directivities. In this class of events about one-quarter of the total nuclear charge emerges as intermediate-mass fragments with nuclear charges $Z > 2$. These fragments are centered at midrapidity and are produced with large transverse velocities.

PACS numbers: 25.70.Pq

Earlier studies [1,2] of heavy-ion collisions at incident energies between 0.1A and 2A GeV have shown that several requirements should be met in order to extract information about the properties of nuclear matter at high temperatures and densities: (1) The system should be as large as possible, (2) the collision geometry needs to be well characterized, and (3) a large number of different observables should be measured simultaneously in order to resolve existing ambiguities in the theoretical interpretation. In particular, theoretical studies [3–5] have shown that *combining* high-precision information on the single-particle momentum-space distributions with global observables characterizing collective flow could be a powerful tool to unravel the effects caused by the collective mean field from those generated by individual elementary hadron-hadron collisions. Recently, large collective flow was observed to be preferentially associated with intermediate-mass fragments (IMFs, $3 \leq Z \leq 10$) [6]. However, their origin and production mechanism are not yet understood and currently are the object of intensive experimental research [7–11]. Momentum-space distributions under exclusive conditions are necessary to clarify the possible sources of these fragments and their comparison with theory may shed some light on the underlying collision dynamics.

The system Au+Au has been studied at an incident energy of 150A MeV and in this Letter, we present, for the first time in this mass and energy regime, invariant cross sections $(1/p_t)d^2\sigma/dp_t dy$ in the plane of rapidity versus transverse momentum per nucleon ("rapidity plot": y vs p_t/A, where A is the fragment mass) for intermediate-mass fragments of identified charge. Our interest is focused on collisions with small impact parameters because in this case the largest participant zone is involved, the longest possible time is spent under heated and compressed conditions, and the flow of particles is least likely to be hampered by spectator material. To select high-centrality events, a novel method was used: In

addition to high charged-particle multiplicities [12], small transverse-momentum directivities [13,14] are also required and this sorts out an event class where most of the yield of intermediate-mass fragments is centered at midrapidity. In fact, due to fluctuations, a selection based on multiplicity alone is not effective enough at this incident energy. As known experimentally, in noncentral collisions [13,14] collective phenomena result in an azimuthal alignment of the emerging particles. Taking the argument the other way, the azimuthal balance of the transverse momenta can be used as a definition of central collisions. The advantage of this approach is that the momentum distributions of the single particles as well as their abundance are not a trivial consequence of the selection criterion and can be used to characterize the collision and possible sources.

Applying this double selection cut, we find a source of intermediate-mass fragments centered at midrapidity with a total multiplicity of $\langle M_{\mathrm{IMF}}\rangle \approx 4$ (in our acceptance). This is a rather remarkable fact in view of the energy of $37A$ MeV available in the center-of-mass system. This central rapidity component is visible even for fragments as heavy as nitrogen and exhibits large transverse-momentum values.

The data were taken with the newly built FOPI detector system at the rapid-cycling synchrotron SIS in Darmstadt, Germany. For the first measurement the system Au+Au was chosen at an incident energy of $150A$ MeV because of the sizable production rate of heavier IMFs, the larger transverse flow, and the predicted weak influence of momentum-dependent forces on the extraction of the compressibility constant. Currently the so-called phase I of the FOPI project consists of a highly granular plastic scintillator wall with altogether 764 elements, each of them providing an energy-loss and a time-of-flight signal, spanning laboratory polar angles of $1° \leq \Theta_{\mathrm{lab}} \leq 30°$ with full azimuthal coverage. In order to achieve low detection thresholds a shell of energy-loss detectors (188 elements) is mounted in front of the scintillators behind a He bag. The system allows element identification of $Z < 15$ particles with detection thresholds increasing from $14A$ to $50A$ MeV as Z increases from 1 to 15. The forward wall is complemented by movable small-solid-angle Si-CsI telescopes ($\Delta\Omega = 20$ msr) extending the polar-angle coverage to $\Theta_{\mathrm{lab}} \leq 65°$. Details about the apparatus will be given elsewhere [15].

A target of 0.5% interaction length (200 mg/cm^2) was irradiated with beam intensities of up to 2×10^5 particle/s, keeping the pileup and the double-hit probability below 1% and 5%, respectively. 10^6 events were taken triggering on the charged-particle multiplicity in the angular range of $7° \leq \Theta_{\mathrm{lab}} \leq 30°$. The multiplicity distribution is shown in Fig. 1 (solid line) after subtraction of background obtained from the comparison of measurements with (dotted line) and without (dash-dotted line) target.

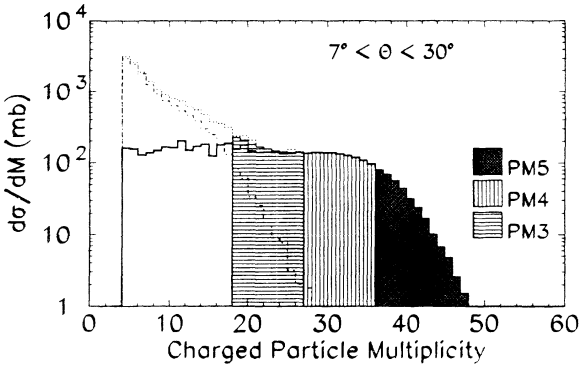

FIG. 1. Charged-particle multiplicity distribution for target-in (dotted line) and target-out (dash-dotted line) measurements. The solid histogram gives the background-subtracted distribution with the selection cuts indicated by differently hatched areas (PM3–PM5).

The multiplicity distribution shows the typical flat plateau and falls off steeply to higher multiplicities. A reasonable highest-multiplicity cut (PM5 with the limit $L_{\mathrm{PM5}} = 36$) starts at half of the plateau value [6] corresponding to an integrated cross section of 350 mb and a maximum impact parameter of 3.3 fm in a sharp-cutoff approximation. The rest of the multiplicity range is then subdivided into four equally spaced intervals. In the following we focus on the description of the semicentral and central events (PM3–PM5), where background contributions amount to a maximum of 14% at PM3 and are therefore negligible. For these event classes the apparatus was able to identify on the average fifty charge units of all the particles emitted into the forward hemisphere of the center-of-mass system.

The second selection step is illustrated in Fig. 2, displaying the distribution in transverse-momentum directivity for the events in the three highest multiplicity

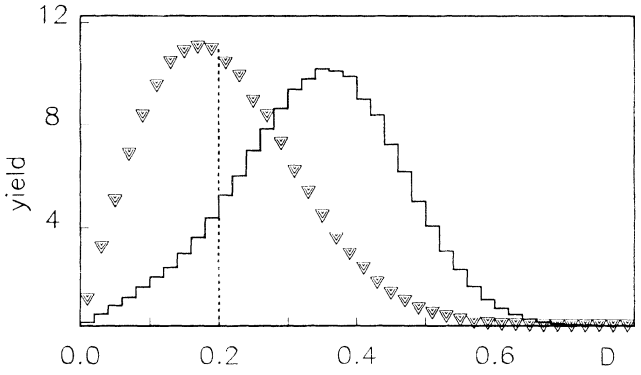

FIG. 2. Distribution of transverse-momentum directivity (D) for the combined upper three multiplicity bins shown in Fig. 1. The result of an azimuthal randomization of the particles is represented by triangles; the indicated cut at $D = 0.2$ is used in the further analysis.

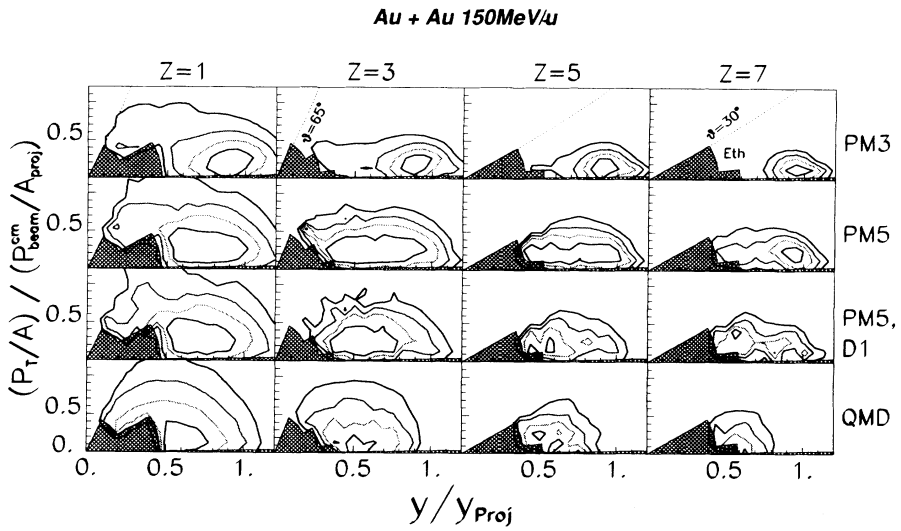

FIG. 3. Experimental rapidity plots (upper three rows) for H, Li, B, and N under different global selection criteria explained in the text. The lowest row represents QMD calculations [16] for small impact parameters ($b \leq 1$ fm). The contour lines represent linear cuts in the invariant cross section at a 20%, 40%, 60%, and 80% level. The solid lines indicate the detector angle boundaries in this representation, while the hatched areas represent the energy detection thresholds. Data at $\theta \geq 30°$ were measured by the telescopes and are presented, due to statistical limitations, only for H and Li.

bins. Transverse-momentum directivity D is defined by

$$D = \frac{|\Sigma_i \mathbf{p}_t|}{\Sigma_i |\mathbf{p}_t|}\Bigg|_{y_i \geq y_{c.m.}}.$$

The sums extend over all identified charged particles with $Z \leq 15$ in one event, having longitudinal momenta pointing forward in the center-of-mass system. The momenta were calculated assuming $A = 2Z$. Experimentally it has been observed [14] that the mean value of the distribution is shifted towards larger values than expected from random-walk considerations. This fact is confirmed by our data and made evident in the figure by comparison with the distribution (triangles) obtained for the same events by randomizing event-wise the azimuthal emission angles. This latter distribution is expected to be more representative of the most central events where no preferential azimuthal emission should exist. The adopted cut $D \leq 0.2$ (henceforth called D1) should therefore enhance centrality.

The dependence of the IMF production on our centrality selection criteria is displayed in Fig. 3 in terms of rapidity plots for four different elements. For easier readability, the rapidity and the transverse momentum per nucleon are presented in units of the projectile rapidity and of the beam momentum per nucleon (in the c.m. system), respectively. Several trends are found in the data: As the multiplicity is increased (PM3 → PM5) the yield is shifted from the spectator region towards midrapidity. In the bin PM5 this results in an almost flat distribution for H, Li, and B, while for heavier fragments a strong spectator component is still visible. More severe restrictions on the charged-particle multiplicity have little effect on these distributions. Sorting out the events with the smallest directivities (PM5,D1) reduces the data sample to 16% (56 mb, 5800 events) and gives rise to the rapidity plots in the third row of Fig. 3 with an integrated yield of (134, 14, 3.2, and 0.9) $\times 10^3$ entries for $Z = 1$, 3, 5, and 7, respectively. As compared to PM5, a substantial shift towards midrapidity is observed, especially of the heavier IMFs, strongly suggesting the presence of a midrapidity source for fragments as heavy as N ($Z = 7$). This also demonstrates the increased sensitivity obtained by measuring IMFs since the distributions for H in the bins PM5 and PM5,D1 are nearly indistinguishable. Although they also seem to be centered at midrapidity, their width is much larger and complete stopping of the incident nuclei can be inferred much more clearly from the IMF invariant cross sections. The fact that heavy IMFs play such a dominating role is very interesting in itself. The observed integral average IMF multiplicity (in our acceptance) is rather independent of the centrality and contributes to about one-quarter of the totally emitted charge ($\langle M_{IMF} \rangle = 3.8$, 4.1, and 3.8 for the bins PM3, PM5, and PM5,D1, respectively). However, strong changes can be observed in the momentum space distributions, thus demonstrating the importance of complete differential measurements.

A more quantitative understanding of the observed behavior and the link to basic nuclear matter properties can only be reached by comparison with theoretical calculations [3–5,16]. However, this is meaningful only for models which can be used as event generators, so that the experimental filter can be easily applied to the theoretical

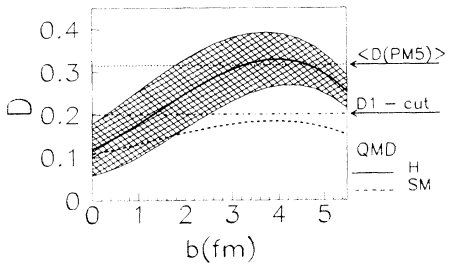

FIG. 4. Impact-parameter dependence of directivity D for two different QMD calculations [16]: H (solid line) and SM (dashed line). The arrows give the experimental average value of D in the multiplicity bin PM5 and the adopted cut D1, respectively.

results. This requirement is met by a quantum molecular dynamics (QMD) code [16] which was made available to us. Depicted in Fig. 4 are the results for two different scenarios: "SM" makes use of a soft equation of state (EOS) with $K=200$ MeV and a momentum-dependent interaction; "H" models a compressibility of $K=380$ MeV (hard EOS). In both cases nucleon-nucleon scattering cross sections as obtained from nonrelativistic g-matrix calculations were used [16,17]. The already mentioned selectivity of the D cut based on the existence of directed flow can be inferred from Fig. 4. Here the mean value of the D distribution in the PM5 bin is presented as a function of the impact parameter for a stiff (solid line) and a soft (dashed line) EOS; the widths of the distributions are similar in the two cases and therefore it has only been indicated for the stiff EOS (hatched area). The soft-EOS calculation fails to reproduce the average value of D seen in the data, and it also fails to explain the selectivity of the directivity observable; cutting at any value of D would not enhance small impact parameters. On the contrary, the hard-EOS results in a strong variation of the mean value of D, ranging from the experimentally observed mean value down to the statistical limit for independent particle emission (see Fig. 2). Therefore, the comparison of data and calculations currently favors a stiff EOS, although it should be kept in mind that an *increased* in-medium cross section could produce collective flow as well [16]. At an incident energy of $150A$ MeV momentum-dependent forces are, however, at least in the framework of the nonrelativistic QMD model, not strong enough to produce the observed flow. Quantitatively, there are nevertheless differences between data and theory even for the hard-EOS calculations, namely, the absolute value of D is still underestimated and the emission patterns for central collisions differ in detail. For a meaningful comparison, central collisions ($b \leq 1$ fm) were selected in the calculation (a relativistic simulation of the experimental selection criteria is hindered by computing time limitations) and are plotted in the lowest row of Fig. 3. The general features of stopping and the substantial IMF production (the model predicts $\langle M_{\mathrm{IMF}}^{\mathrm{QMD}} \rangle \approx 4.8$) are nicely reproduced, but the p_t/A spectra at midrapidity do not exhibit the common transverse velocity that seems to be present in the data; i.e., the observed transverse momenta of the IMFs at midrapidity are larger than those from the QMD calculation and by far exceed those of any thermal model. Certainly more systematic comparisons with the calculations are needed.

In summary, exploiting the full azimuthal coverage of the FOPI detector system, small directivity in the forward hemisphere of the c.m. system can be used to better select central collisions. The selection mechanism gives rise to momentum space distributions that are centered at midrapidity for fragment masses up to $A=14$ with large transverse velocities. The selection mechanism is currently only reproduced by QMD calculations making use of a stiff EOS.

We are much indebted to the technical staffs at the different institutes for the very essential support in implementing the FOPI detector and to the SIS accelerator staff for the delivery of an excellent Au beam. The authors would like to thank J. Aichelin for the use of the QMD code as well as for many clarifying discussions.

[1] R. Stock, Phys. Rep. **135**, 259 (1986).
[2] H. Gutbrod *et al.*, Rep. Prog. Phys. **52**, 1267 (1989).
[3] G. Peilert *et al.*, Phys. Rev. C **39**, 1402 (1989).
[4] V. Koch *et al.*, Nucl. Phys. **A532**, 715 (1991).
[5] A. Lang *et al.*, Z. Phys. A **340**, 287 (1991).
[6] K. G. R. Doss *et al.*, Phys. Rev. Lett. **59**, 2720 (1987).
[7] Y. Blumenfeld *et al.*, Phys. Rev. Lett. **66**, 576 (1991).
[8] S. J. Yennello *et al.*, Phys. Rev. Lett. **67**, 671 (1991).
[9] C. A. Ogilvie *et al.*, Phys. Rev. Lett. **67**, 1214 (1991).
[10] D. R. Bowman *et al.*, Phys. Rev. Lett. **67**, 1527 (1991).
[11] R. T. Souza *et al.*, Phys. Lett. **B268**, 6 (1991).
[12] K. G. R. Doss *et al.*, Phys. Rev. C **32**, 116 (1985).
[13] P. Beckmann *et al.*, Mod. Phys. Lett. A **2**, 163 (1987).
[14] R. Bock *et al.*, Mod. Phys. Lett. A **2**, 721 (1987).
[15] A. Gobbi *et al.* (to be published).
[16] J. Aichelin, Phys. Rep. **202**, 233 (1991); (private communication).
[17] N. Ohtsuka *et al.*, Nucl. Phys. **A465**, 550 (1987).

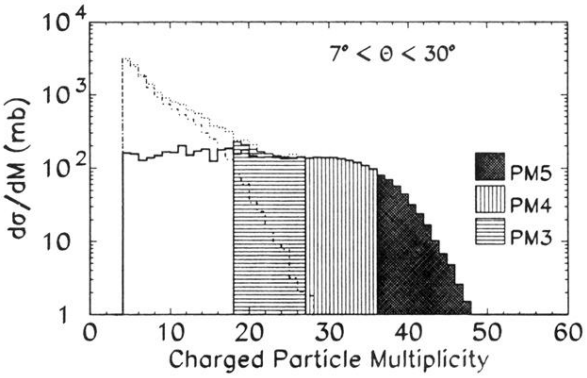

FIG. 1. Charged-particle multiplicity distribution for target-in (dotted line) and target-out (dash-dotted line) measurements. The solid histogram gives the background-subtracted distribution with the selection cuts indicated by differently hatched areas (PM3–PM5).